THE JOURNAL OF PHYSICAL CHEMISTRY C

Article

pubs.acs.org/JPCC

Adsorption of Ethanol Vapor on Mica Surface under Different Relative Humidities: A Molecular Simulation Study

Tao Cheng and Huai Sun*

School of Chemistry and Chemical Engineering and Key Laboratory for Thin Film and Microfabrication of Ministry of Education, Shanghai Jiao Tong University, Shanghai 200240, China

Supporting Information

ABSTRACT: The adsorption of ethanol vapor on a mica surface at 298 K and different relative humidities (RHs) are studied using grand canonical Monte Carlo and molecular dynamics simulations. The simulations show that the adsorbed ethanol molecules form a monolayer on the mica surface, sharply contrasting the behavior of water, which forms multiple adsorption layers on the mica surface. Simulations of an ethanol and water mixture reveal that the adsorbed molecules are segregated into a water-rich domain near the mica surface and an ethanol-rich domain on top of the water-rich domain. The water-rich domain exhibits multilayers unless the RH is extremely low (<1%), whereas the ethanol-rich domain exhibits a monolayer. These findings are supported by calculations of the isosteric heats of adsorption and analyses of configurations, concentrations, and diffusivities of molecules in different layers.

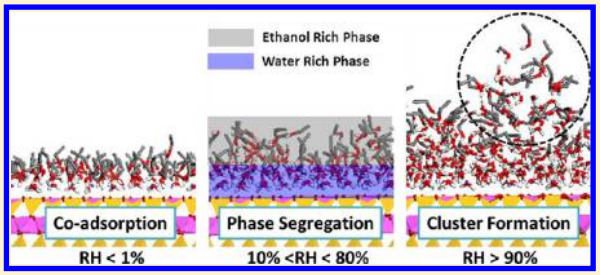

1. INTRODUCTION

Mica is a natural clay with a sandwiched structure that can be easily cleaved into a flat surface. This character makes mica one of the most studied materials, both experimentally and theoretically. The interfacial phenomena of mica, particularly the structures of water molecules adsorbed on it, have been extensively studied.[1−22] In 1997, Hu et al.[3] studied water thin films on mica surface using scanning polarization force microscopy (SPFM) and observed the formation of thin islands of molecules with contact angles of 120° at the boundary; the authors thus proposed the ice-like structure of water on mica. Since then, several investigations have been reported to support the existence of this ice-like structure both experimentally and theoretically.[4,6−9,11] Unfortunately, no direct evidence has yet been found to confirm the ice-like structure of water on mica due to limitations in equipment resolution. However, all of the studies thus far acknowledge that water possesses ordered structures on mica surfaces. Pioneering Monte Carlo (MC) simulations of water on mica were conducted by Delville,[23] who focused on adsorption at different relative pressures and found that the predicted adsorption amount is significantly lower than the experimental data; this discrepancy could be attributed to the inaccuracy of the force field used. A new general clay force field (CLAYFF)[24] that reproduces the structure and mechanical properties of common clays, including mica, has recently been reported. Combining the CLAYFF and Simple Point Charge (SPC) water models, Malani and Ayappa[25] reproduced an experimental adsorption curve of water on mica using MC simulations. Although these authors did not observe ice-like structures, they found that water molecules are highly restricted on the mica surface, particularly those adjacent to the mica surface. Similar results were also obtained from the molecular dynamics (MD) simulations conducted by Wang et al.,[14] who found that water molecules are structurally restricted at the adsorption sites. Extending these simulations to include a larger amount of water of up to seven to eight molecular dimensions on the mica surface, Wang also reported that water demonstrates a bulk-like configuration above the surface by three to four molecular dimensions. The existence of this bulk-like configuration is consistent with a recent XRD experiment.[9]

Most of the works related to mica surfaces have focused on pure substance. Adsorption of a mixture on the mica surface is of great interest to learn because the different interactions of molecules may provide a unique opportunity for modulating surface properties.[26−34] Fang et al.[35] reported the transition of DNA structures induced by a water/ethanol mixture. They observed a transition of DNA molecules from all-B-forms to all-A-forms by varying the ethanol concentration. Another interesting work reported by Zhang et al.[36] showed that λ-domain DNA can be condensed by rinsing with an ethanol/water mixture. Mica surfaces are stable and well understood; thus, studies of ethanol/water mixtures on mica surfaces would be an ideal case to understanding the adsorption of mixtures. However, characterizing the adsorption of mixtures using experimental methods is highly challenging. To this end, computer simulations provide the potential to study interfaces at atomistic level.

In this work, simulations were carried out using the grand canonical Monte Carlo (GCMC) and Molecular Dynamics MD

Received: March 1, 2012
Revised: July 8, 2012
Published: July 14, 2012

dx.doi.org/10.1021/jp3020595 | J. Phys. Chem. C 2012, 116, 16436−16446

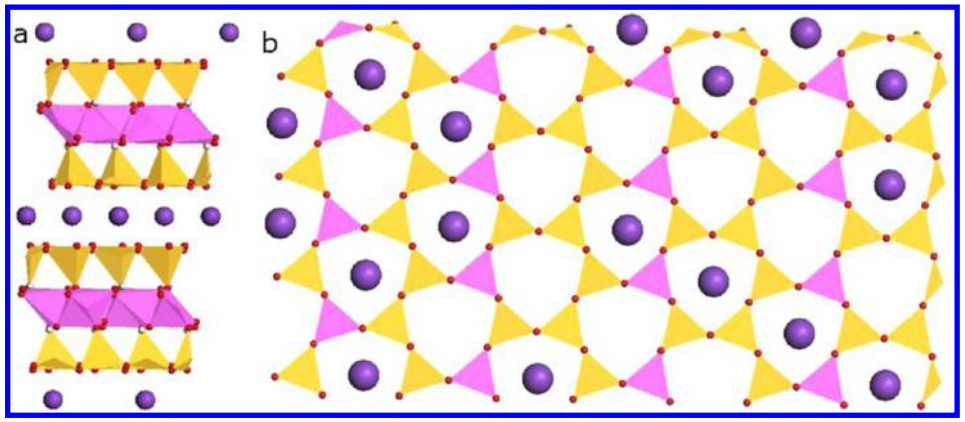

Figure 1. Mica structure used in this work: (a) side view and (b) top view. Colored balls represent K^+ in purple, O in red, and H in white. The polyhedron contains silicon and aluminum at the center: the yellow polyhedron is silicon at the center, and the pink polyhedron is aluminum at the center.

methods to study the adsorptions of ethanol under different relative humidities (RHs) on mica surfaces. Simulations of pure water and ethanol on the mica surface were conducted for comparison to understand the adsorption of the mixture under different RHs. Our simulations reveal two novel findings: (1) The ethanol adsorption exhibits a monolayer on the mica surface while water adsorption exhibits a multilayer. (2) For the mixtures, the adsorbates are segregated into a multilayer water-rich domain covered by a monolayer ethanol-rich domain on the surface. In the following sections, the simulation process will first be explained, followed by the simulated results and discussions and comparisons with known experimental and computational work. Finally, the conclusion is presented.

2. SIMULATION DETAILS

The X-ray structure data of muscovite mica reported in the literature[37] was used as the mica model (Figure 1). Mica has a sandwich-like layered structure consisting of one aluminum layer between two silicate layers. In each of the silicate tetrahedral sheets, one silicate is substituted by aluminum every four silicate sites. As a result, half of the six-member rings have Si_4Al_2 composition, while the other half is composed of Si_5Al_1; no Al−O−Al bonds are allowed in the structure. All tetrahedral Al atoms in our muscovite model were arranged in an ordered fashion for simplicity, similar to that of a previous simulation work.[14] A freshly cleaved mica surface has an oxygen surface layer with a random distribution of K^+ ions. In the simulations, one K^+ ion from each unit cell was removed (with equal probability) to create a random distribution of K^+ ions on the mica surface, similar to that of a previous simulation work.[25] The mica surface consisted of $9 \times 6 \times 1$ unit cells, making up a periodic cell of lateral dimensions L_x = 4.686 nm and L_y = 5.41 nm. The simulation cell was built such that the x−y plane of the simulation cell represented the mica surface and the z-axis was normal to the mica surface. The 3-D periodic boundary condition was applied with the simulation box. The cell height was 31.813 nm, including 1.813 nm for the mica slab, and 30.0 nm for the vapor space. The vapor space was long enough to eliminate the periodic image interactions. Three types of adsorbates, namely, water vapor, ethanol vapor, and ethanol vapor under various RH (water), were considered in this work. Figure 2 shows snapshots of the three interface systems.

The force field was selected as follows. Water was represented by the SPC three-site water model,[38] and ethanol

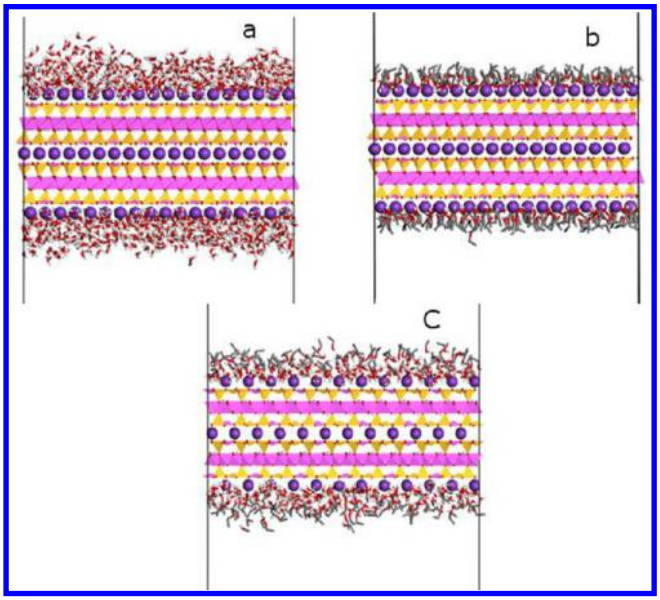

Figure 2. Snapshots of the GCMC simulation of (a) water/mica, (b) ethanol/mica, and (c) their mixture (ethanol under different RH)/mica interfaces. The colored balls and polyhedrons are the same as explained in Figure 1.

was represented by the TraPPE united atom force field.[39] The combination of SPC water with TraPPE-UA ethanol was validated by Lundsgaard et al.[40] Mica was described by CLAYFF potential parameters, which have been successfully used to study the swelling of clays and the structure of water on muscovite mica using MD simulations.[24] The framework of mica and the positions of K^+ ions were fixed, similar to that of a previous simulation work.[25] The total energy between the mica and adsorbed molecules included Lennard-Jones (LJ) and electrostatic interactions. The 12-6 LJ potential between two sites i and j was

$$U_{ij} = 4\varepsilon_{ij}\left[\left(\frac{\delta_{ij}}{r_{ij}}\right)^{12} - \left(\frac{\delta_{ij}}{r_{ij}}\right)^{6}\right] \quad (1)$$

where, ε_{ij} and σ_{ij} are LJ parameters. Lorentz−Berthelot mixing rules were used to calculate ε_{ij} and σ_{ij} for unlike sites.

$$\varepsilon_{ij} = \sqrt{\varepsilon_{ii}\varepsilon_{jj}} \quad (2)$$

dx.doi.org/10.1021/jp3020595 | J. Phys. Chem. C 2012, 116, 16436−16446

$$\delta_{ij} = \frac{\delta_{ii} + \delta_{jj}}{2} \quad (3)$$

Electrostatic energies were described using Columbic interactions of atomic partial charges.

GCMC (constant μVT) simulations were carried out to study the adsorptions on the mica surface.[41] Chemical potentials of both water and ethanol were calculated using the Widom insertion method with NPT MC simulations. The calculated chemical potential of water at saturated vapor pressure was −5446 K, which is consistent with that reported by Liu and Monson.[42] The calculated chemical potential of ethanol at saturated vapor pressure was −3438 K. Assuming that the vapor is an ideal gas, the chemical potential at different relative pressures (μ) may be estimated using the following relationship:[25]

$$\frac{p}{p_0} = \frac{e^{\mu/k_B T}}{e^{\mu_0/k_B T}} \quad (4)$$

where μ_0 is the chemical potential at saturated vapor pressure P_o, k_B is the Boltzmann constant, and T is the temperature. Each GCMC simulation was performed for 2×10^8 equilibration moves, followed by 1×10^8 production moves, during which the ensemble-averaged properties were evaluated. Each move consisted of insertion or deletion, intrabox exchange of two molecules, configuration-biased molecule regrowth,[43] or displacement accompanied with rotation. Moves were attempted with equal probability. The maximum rotation and displacement of a molecule was modified with a probability of 0.5 (half of the displacement probability) every 1000 moves.

MD simulations were carried out starting from the saturated adsorption configuration generated from the MC simulation to analyze the dynamic properties. All simulations were carried out using GROMACS 4.0.3.[44] The Berendsen weak coupling technique[45] was used to modulate the temperature with relaxation times of 0.1 ps. A time step of 1 fs for the integration of the motion equations was chosen. The particle mesh Ewald technique[46] was used to evaluate electrostatic interactions. A real-space convergence parameter of 3.5 nm was used in combination with a cutoff of 1.0 nm of VDW interactions. The reciprocal space sum was evaluated with a resolution of 0.12 nm. The nonbond list was updated every five steps. The steepest descent method was then used to perform 1000 steps of minimization. This process was followed by equilibration for 100 ps and data collection every 500 ps. Averages of properties and standard deviations were calculated from three independent simulations.

The orientation of the adsorbates on the mica surface is described by calculating the order parameter S,[47] which represents the average angle of a defined vector with respect to a reference vector. In this paper, the z-axis, which is normal to the surface, was used as the reference vector. The S order parameter was calculated using the following formula:

$$S = \frac{1}{2}\langle 3\cos^2\theta - 1\rangle \quad (5)$$

where θ is the angle between the specified vector and the reference vector. The order parameter varied between 1 (perfectly along the reference vector) and $-1/2$ (perfectly perpendicular to the reference vector). However, the averaged S was insensitive to the angle distribution shape. Therefore, the S for molecules in geographically limited regions was calculated.

In addition, distribution patterns were plotted to study the liquid structures when necessary. The mobility of molecules on the surface was evaluated by calculating the 2-dimensional lateral diffusion coefficients using the Einstein relation.

$$\lim_{t\to\infty}\langle \| r_i(t) - r_i(0)\|^2\rangle_{i\in A} = 6Dt \quad (6)$$

The isosteric heat of adsorption, q_{st}, can be evaluated using energy and particle fluctuations in the grand canonic ensemble,[48]

$$q_{st} = -\frac{\langle N_w U\rangle - \langle N_w\rangle\langle U\rangle}{\langle N_w{}^2\rangle - \langle N_w\rangle\langle U\rangle} + k_B T \quad (7)$$

where N is the total number of adsorbed molecules and U is the total energy consisting of interactions among the adsorbed molecules, and interactions of adsorbed molecules and adsorbent.

3. RESULTS AND DISCUSSION

3.1. Water on Mica Surface. The simulated adsorption isotherm for water vapor on mica at 298 K is shown in Figure 3.

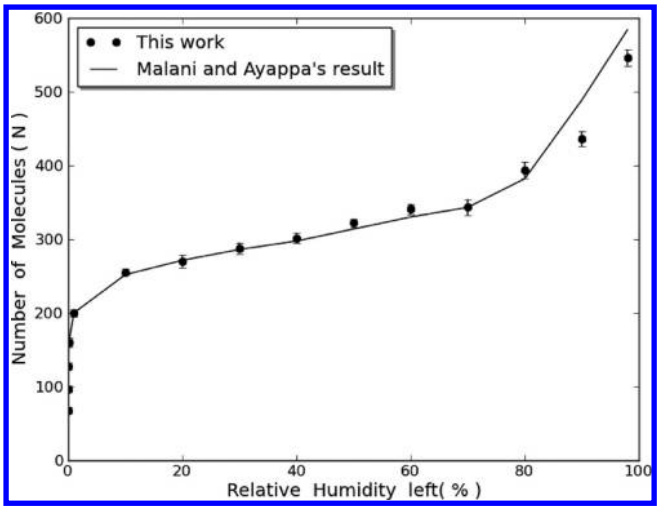

Figure 3. Comparison of simulated adsorption isotherms of water on mica at 298 K between this work (dots with error bars) and that of Malani and Ayappa.[25] (line).

The simulated data of Malani and Ayappa.[25] are also shown in the same figure for comparison. Based on the IUPAC classification, the isotherm represents a typical type II adsorption. The adsorption amount at low RH (<10%) increases rapidly as the RH increases. A plateau appears between RH = 10% and 80%, and the adsorption increases rapidly again after RH = 80%. The second turning point indicates a transition from monolayer to multilayer adsorption. Our data agree very well with those reported by Malani and Ayappa[25] at RH below 80%. On the other hand, slight deviations are observed at high RH (>80%), which may be due to variations in the simulation models. For instance, K^+ ions are randomly distributed on the surfaces in both the current and previous works.[25]

The same results for pure water adsorbed on the mica surface are obtained compared with those reported previously;[25] thus, structural analysis data are provided in the Supporting Information (SI, Figures S1 and S2). The main features of water vapor adsorbed on the mica surface can be summarized

dx.doi.org/10.1021/jp3020595 | J. Phys. Chem. C 2012, 116, 16436−16446

as follows for the comparisons and discussions presented below. The adsorbed water molecules are distributed in four distinguishable layers (L0 to L3), as shown in Figure S1. Water molecules are only in L0 and L1 at low RH, and the populations extend to L2 and L3 as RH increases. The populations in L0 and L1 are strongly correlated, and the combined total population of L0 and L1 reaches a maximum at approximately RH = 10%. The distance between the L0 and L1 is less than one molecule dimension (0.3 nm), whereas the distance between the surface to L1 is about one molecular dimension. Therefore, L0 and L1 make up one adsorption layer as specified by IUPAC terminology.[33] The order parameters calculated for water molecules on the surface (Figure S2) show that L0 water adopts a configuration in which two hydrogen atoms interact with the surface oxygen to form two hydrogen bonds, whereas in the L1 configuration, only one hydrogen of water interacts with the surface oxygen, another forms hydrogen bonds with other waters laterally. This configuration also facilitates the hydration of K^+.

Distinguishing between calculated population layers and commonly referred adsorption layers is necessary. According to the IUPAC, a monolayer refers to the surface phase in direct contact with the surface, with thickness not exceeding one molecule in size, whereas a multilayer refers to the subsequently adsorbed layers of adsorbate not in contact with the surface. Therefore, L0 and L1 belong to one adsorption monolayer, because L0 and L1 both directly interact with mica surface, only different in configurations. Thus, L0 and L1 are considered as configurational layers. This definition is used in this paper and is important for understanding the following discussions on the adsorption of ethanol vapor with different RHs.

3.2. Ethanol Adsorption on Mica. The simulated isotherm curve of ethanol vapor on mica surface shown in Figure 4 is very different from that of water vapor (Figure 3). The curve shows a typical IUPAC type I adsorption with a long plateau. The amount of ethanol adsorbed increases rapidly as the relative vapor pressure increases from 0% to 15%. The curvature changes around 10% after the turning point; however, the increment is small until the saturated vapor pressure (100%) is reached. No second turning point is observed in the curve for ethanol, and the maximum number of ethanol molecules adsorbed (~140) is much less than the number (~550) of water molecules adsorbed.

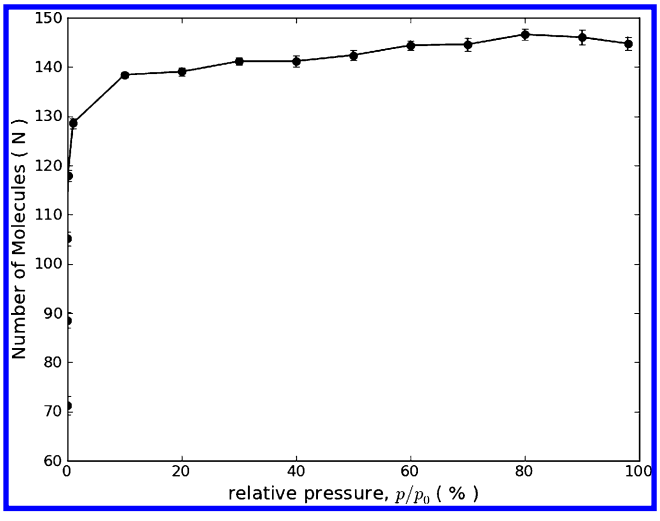

Figure 4. Simulated adsorption isotherm (dots with error bar) of ethanol on mica at 298 K; the trend line is shown for easy viewing. The *x*-axis represents the relative vapor pressure (p/p_0) as a percentage.

Figure 5 shows the density distributions of ethanol as a function of distance from the mica surface, which is represented by the position of the mica oxygen. The curves calculated for different RHs are shifted along the *y* axis for a better view of Figure 5 and the following figures in this paper. Unlike water, only two oxygen (ethanol) peaks (L1 and L2) can be identified. Close examination of the data and comparison with Figure S1 (for water) show that the position of the first peak is slightly above the position of K^+, roughly at the same position of L1 in the water curve, and the second peak is only about 0.1 nm from the first. Both L1 and L2 are within one molecular dimension (ca. 0.4 nm) from the surface; therefore, both belong to one adsorption monolayer. Figure 5 also shows changes in the populations of molecules in L1 and L2 as the p/p_0 ratio increases. L1 is first taken at very low load, after which L2 is populated as the p/p_0 ratio increases. The position of L1 does not change as the vapor pressure increases; but the L2 peak shifts slightly to the right as the pressure increases.

L1 and L2 represent two different configurations of the adsorbate. Figure 6 shows the order parameters calculated between the H−O bond of ethanol and the *z*-axis (normal to the surface) of the simulation box. The *S* factors are averaged in 500 blocks along the *z* coordinate, and the value in each block describes the orientation of molecules at different distances from the surface. The *S* parameters are positive between 0.18 and 0.26 nm (L1), and the maximum value is 0.8, indicating an average angle of 21.4° between the O−H bond and the *z*-axis. In this configuration, the ethanol H(O) atom forms a hydrogen bond with the mica surface oxygen, and the O atom ethanol interacts with the K^+ cations. The *S* parameters are negative between 0.26 and 0.45 nm (L2), with a minimum value of −0.2, indicating that the O−H bond is 63.4° relative to the *z*-axis. In this configuration, the ethanol O atom interacts with K^+, and the ethanol H(O) atom forms a hydrogen bond with other ethanol molecules laterally. The S beyond L2 represents molecular orientations in the vapor phase. The values are very noisy but average about 0.0.

Zhuo et al.[49] reported simulating ethanol fluid on a mica surface and showed that a "bilayer" is formed near the vicinity of the mica surface. Close comparison of their data[49] against our data shows that the first layer referred to in their paper corresponds to the L1 in our work and the second layer corresponds to L2. Therefore, the reported "bilayer" is actually one adsorption monolayer but with different configurations, as discussed above. The isotherm curve is a typical type-I adsorption and the distances of L1 and L2 to the surface are within one molecular dimension; thus, the adsorption is called a monolayer with two configurations.

Bilayer adsorption has also been reported by experimental works[50] in which the ethanol film thickness was measured, and the size was nearly double that of the dimension of the ethanol molecule. In these works, the sample (cleaved mica) was immersed in an aqueous ethanol solution for 24 h and then dried before measurement. The authors indicated that the immersion time was long enough to reach equilibrium. Using atomic force microscopy, a tail-to-tail bilayer structure of ethanol was observed. A similar bilayer structure of ethanol was also observed at the fused silica surface using sum-frequency vibrational spectroscopy.[34] The formation of the bilayer structure in the solid−liquid interface is understandable.

dx.doi.org/10.1021/jp3020595 | J. Phys. Chem. C 2012, 116, 16436−16446

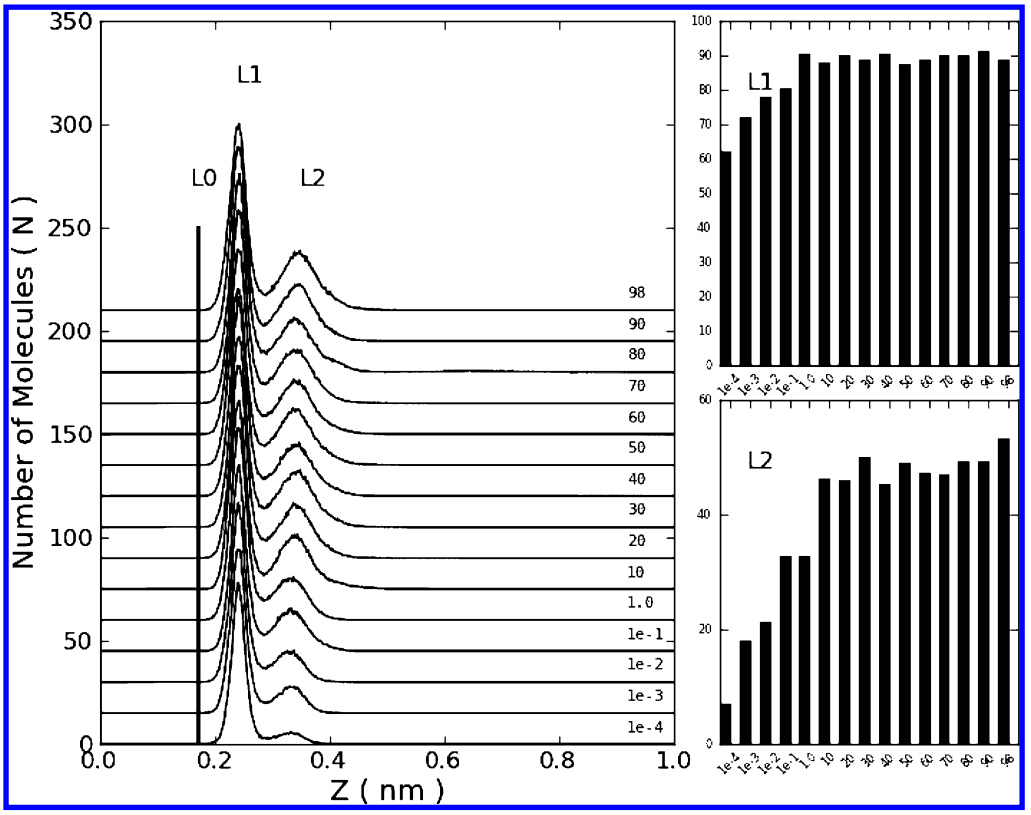

Figure 5. Density distributions of ethanol oxygen as a distance from the mica surface, under various relative vapor pressures (p/p_0 in percentage). The curves calculated at different vapor pressures are shifted along the *y*-axis for better viewing. The *x*-axis represents the distance from the surface identified by the surface oxygen. The solid vertical line indicates the position of K^+. Two peaks, L1 and L2, are identified. No adsorption is observed within L0. The right insets illustrate the population of molecules in layers L1 and L2, as the relative vapor pressure p/p_0 changes.

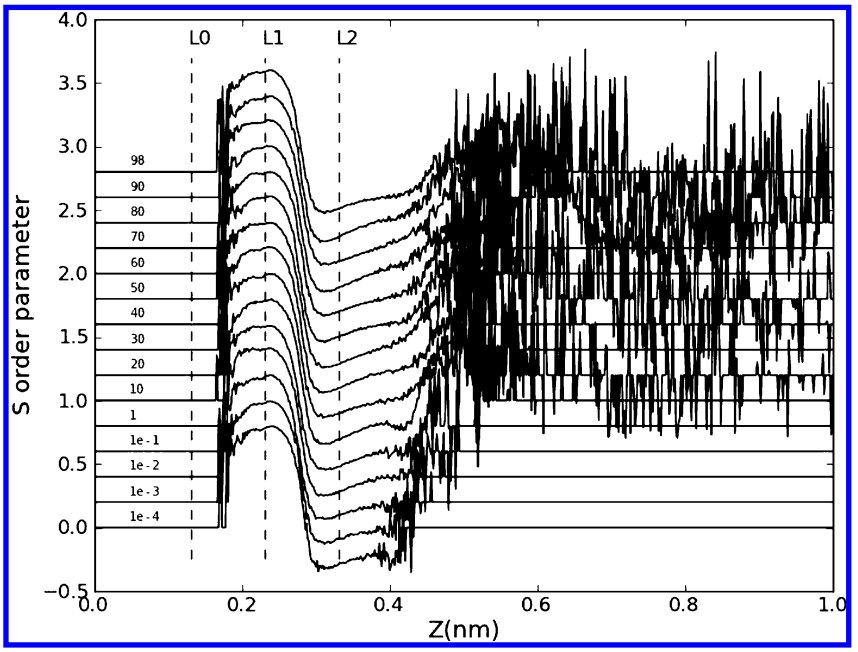

Figure 6. Order parameters (S) between the H−O of ethanol and *z*-axis at different distances from the mica surface and at various relative vapor pressures (p/p_0). $Z = 0$ corresponds to the position of the mica oxygen. The positions L0, L1, L2, and L3 are labeled as dashed vertical lines for viewing convenience. The curves calculated at different vapor pressures are shifted along the *y*-axis for better viewing.

Because the surface is hydrophilic, the ethanol bilayer could be formed in a tail-to-tail configuration so that both hydrophilic sides are in contact with the surface and the water phase. However, the solid−vapor interface is different, only the surface provides hydrophilic interaction. Close examination of our data indicates that the ethyl group of ethanol in L2 faces toward the air, as shown in the snapshot in Figure 2, and additional adsorption is not favored due to the hydrophobic nature of the

dx.doi.org/10.1021/jp3020595 | J. Phys. Chem. C 2012, 116, 16436−16446

ethyl group. Direct measurement of the adsorption of ethanol vapor has yet to be performed on mica surfaces. The most relevant measurements obtained thus far involve the adsorption of ethanol vapor on ice surface at low temperature,[51,52] which demonstrates the monolayer adsorption of ethanol.

Figure 7 shows the calculated isosteric heats of adsorption for pure water and ethanol adsorbed on the mica surface. The

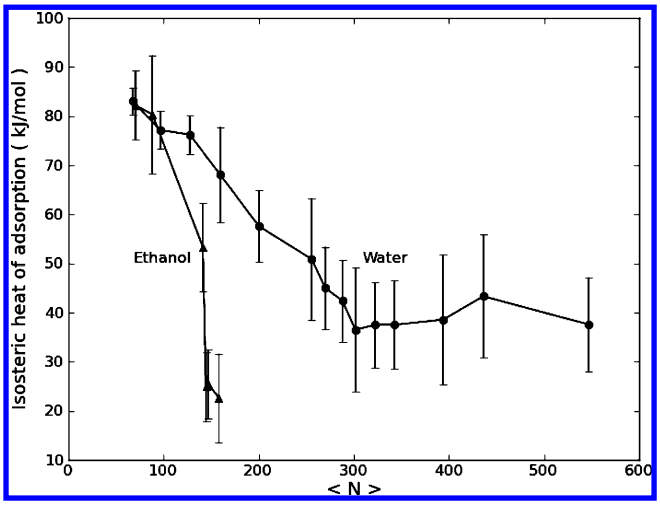

Figure 7. Comparison of the isosteric heats of adsorption (in kJ/mol) for water and ethanol on the mica surface. The *x*-axis shows the number of adsorbed molecules.

initial values for both molecules are almost identical, consistent with the fact that ethanol has an interaction strength similar to that of water on the surface.[51] The calculated values for both molecules decrease as the load increases. However, changes in the curves are significantly different. The heats of adsorption converge to approximately 40 kJ/mol when the amount of water is greater than N = 400, which is close to the heat of vaporization of water (40.65 kJ/mol).[32] The ethanol curve decreases deeply and rapidly as the number of adsorbates increases. The heat of adsorption of ethanol at N = 120 is only approximately 20 kJ/mol, significantly lower than its heat of vaporization (38.6 kJ/mol).[39]

Sharp differences in the isosteric heats of adsorption for water and ethanol provide an explanation of the differences in adsorption mechanisms between these two molecules. The adsorbed molecules for water can still form hydrogen bonds with other molecules; thus, multilayer adsorption occurs and, consequently, the heat of adsorption converges to the heat of vaporization. The hydrogen bonds for adsorbed ethanol are saturated by the mica surface and K^+, and the hydrophobic groups exposed to air do not provide sufficient energy for the second layer adsorption. Consequently, only a monolayer can be formed and the heat of adsorption is much lower than the heat of vaporization of ethanol liquid.

3.3. Ethanol Adsorption on Mica under Different Relative Humidity. Simulated adsorption isotherms for the mixture of ethanol (fixed p/p_0 = 90%) and water (RH varies from 0% to 100%) as function of the RH are shown in Figure 8. The amount of adsorbed ethanol at zero RH is the same as that presented for pure ethanol (Figure 4), wherein about 150 molecules are adsorbed. The amount of ethanol decreases to approximately 75% of the initial amount as the RH increases, and then stabilizes throughout most of the RH range. The amount of ethanol recovers to a value close to 150 as the RH

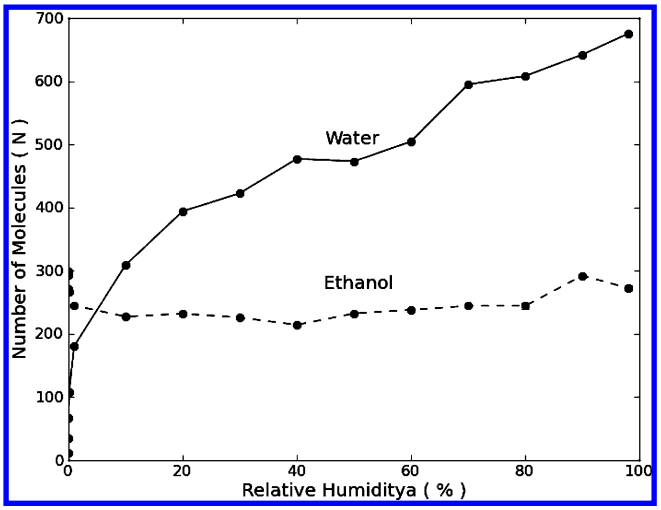

Figure 8. Simulated adsorption amounts of ethanol (dash line) and water (solid line) under different relative humidities on mica at 298 K. The relative vapor pressure of ethanol is fixed at p/p_0 = 90%.

reaches 90%. The amount of adsorbed water increases monotonically as the RH increases, reaching 345 at RH = 100%. However, the curve is quite different from that of pure water (see Figure 3), and the total amount of water adsorbed is significantly lower than that obtained in pure water adsorption.

Analysis of the distributions of these two molecules on the surface reveals the adsorption mechanism. Figure 9 shows the

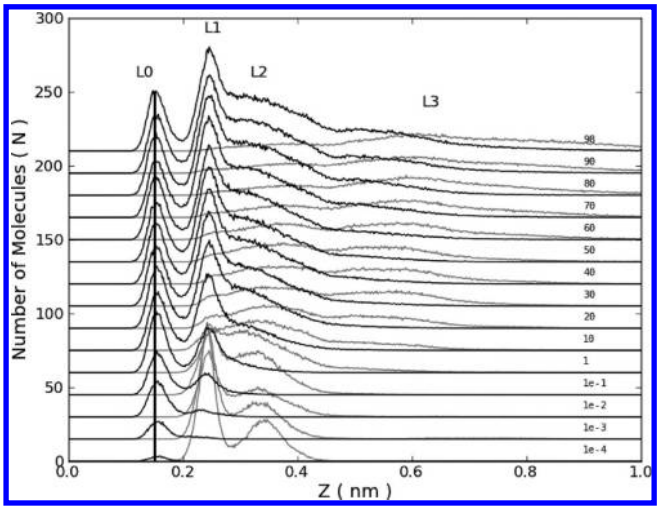

Figure 9. Density distributions of water oxygen (black) and ethanol oxygen (gray) as functions of distance from the mica surface and at different RH. The relative vapor pressure of ethanol is fixed at p/p_0 = 90%. Z = 0 represents the position of the surface oxygen. The solid vertical line indicates the position of K^+. L0, L1, L2, and L3 indicate the molecular population peaks along the z direction.

density distributions of water and ethanol as functions of distance from the surface and at various RH. Two strong peaks (L1 and L2) of ethanol similar to those observed in the pure ethanol case are formed and a small peak (L0) of water at the same position as K^+ is visible at very low RH (<0.01%). The height of the water peak (L0) increases as the RH increases and a second peak of water (L1) develops. Meanwhile, the heights of the two ethanol peaks decrease. Eventually, the first ethanol peak disappears and merges into the second, forming a new peak at L3 at roughly RH = 10%. The water population

dx.doi.org/10.1021/jp3020595 | J. Phys. Chem. C 2012, 116, 16436−16446

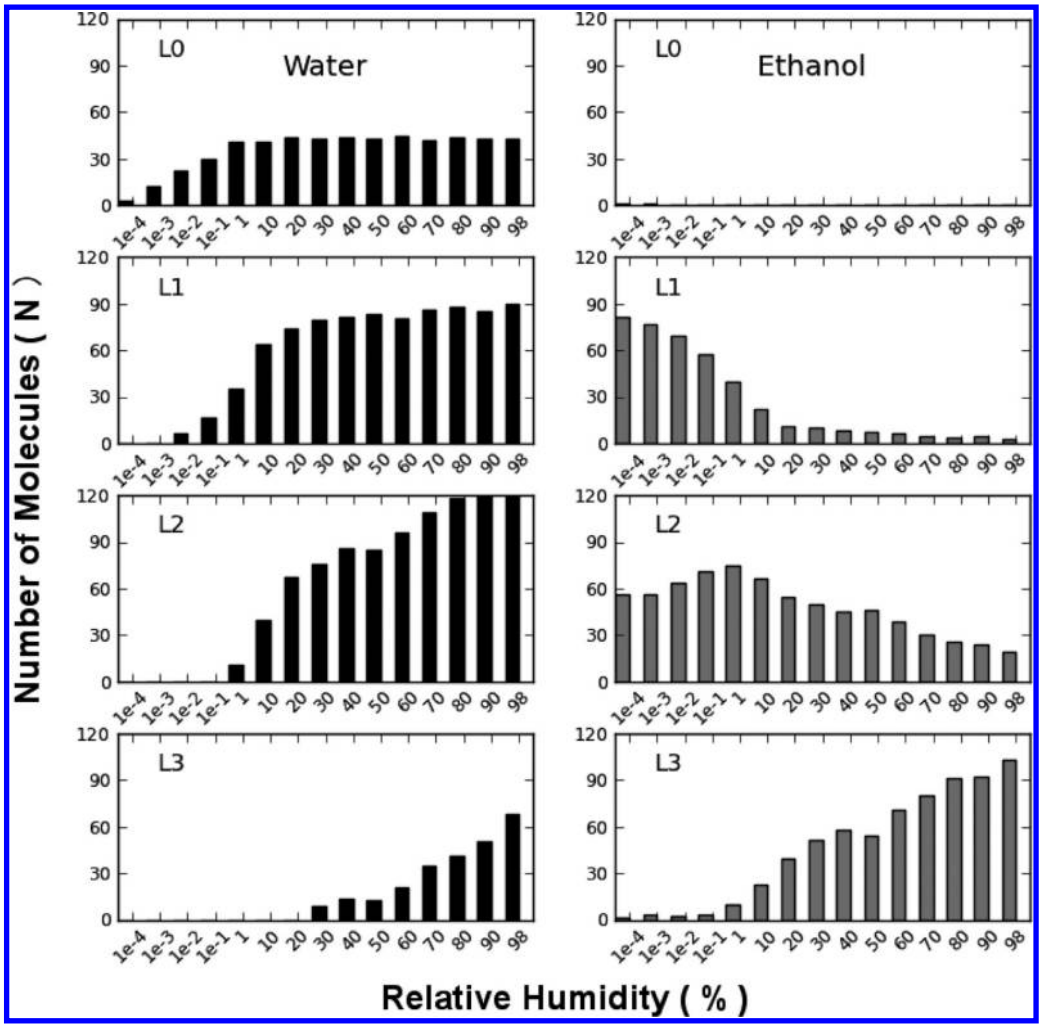

Figure 10. Approximated populations of water molecules (left) and ethanol molecules (right) in layers L0, L1, L2, and L3 (as shown in Figure 9) as functions of RH.

increases as the RH continues to increase. A broad distribution of water beyond the two peaks extends to the right (L2 and L3), in addition to the two sharp peaks (L0 and L1). The distribution of ethanol becomes a broad peak maximized at L3 at very high RH. Using the dimension criterion mentioned above, L0 and L1 forms one adsorption layer, and L2 and L3 belong to different adsorption layers.

The populations of water and ethanol in the four layers are calculated and listed in Figure 10. L0 is accessible only by water, and it is saturated as RH increases to 1%. L1 is the closest layer that ethanol can reach. However, ethanol molecules are gradually replaced by water molecules in L1 as RH increases. A similar trend is seen for L2. The population of ethanol in L2 reaches a maximum at approximately RH = 1% and then decreases. The population of both molecules in L3 increases as the RH increases. The data show that the adsorbates are divided into water-rich and ethanol-rich domains. The water-rich domain at lower RH is L0 and L1, whereas the ethanol-rich domain is L2 and L3. The water-rich domain extends from L0 to L2 at high RH, whereas the ethanol-rich domain is in L3. The two molecules mix at different concentrations in the different domains. The mole fractions of the two molecules in the two domains at RH = 10% and RH = 80% are shown in Table 1.

Table 1. Mole Fractions of Water and Ethanol in Water-Rich and Ethanol-Rich Domains at RH = 10% and RH = 80%

	water-rich	ethanol-rich
RH = 10%	L1 + L2	L3 + L4
$x(w)$	0.83	0.33
$x(e)$	0.17	0.67
RH = 80%	L1 + L2 + L3	L4
$x(w)$	0.89	0.31
$x(e)$	0.11	0.69

The averaged order parameters (S) between the H−H vector of water and the z-axis as function of distance from the surface are shown in Figure 11. The S parameter is similar to that obtained for pure water vapor on the mica surface, as shown in Figure S1. The value is close to −0.5 between 0.1 and 0.2 nm (L0), indicating a configuration where the H−H vector is parallel to the surface. The S order parameter is ca. 0.39 between 0.2 and 0.3 nm (L1), indicating a configuration where the average angle between the H−H vector and the z-axis is about 30°.

The two configurations of water in direct contact with the mica surface are illustrated in Figure 12. Configuration S0 represents molecules in L0, and configuration S1 corresponds

dx.doi.org/10.1021/jp3020595 | J. Phys. Chem. C 2012, 116, 16436−16446

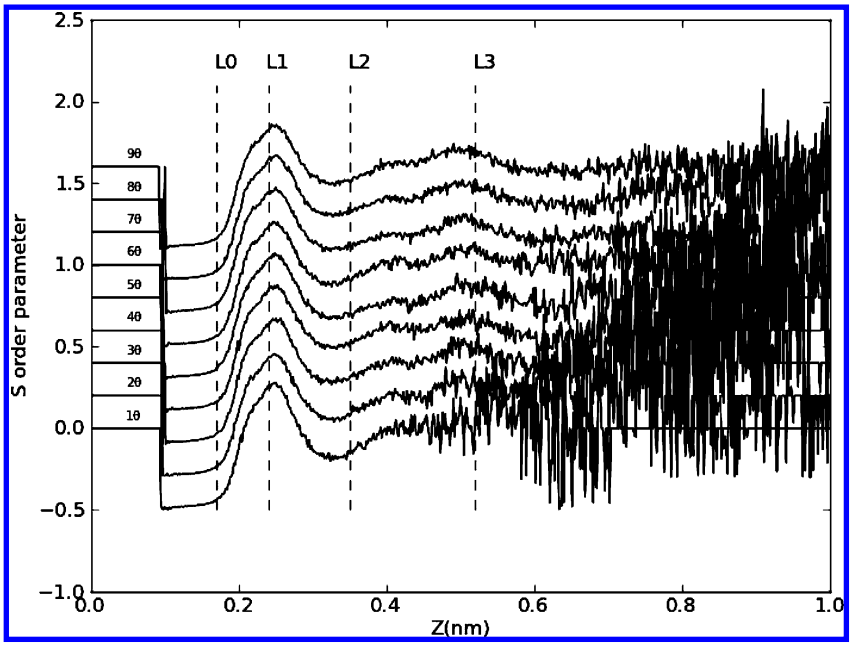

Figure 11. Order parameters between the H−H of water and the *z*-axis as a function of distances from the surface at various RH between 10% and 90%. The positions of L0, L1, L2, and L3 are labeled as dashed vertical lines for viewing convenience. The curves calculated at different vapor pressures are shifted along the *y*-axis for better viewing.

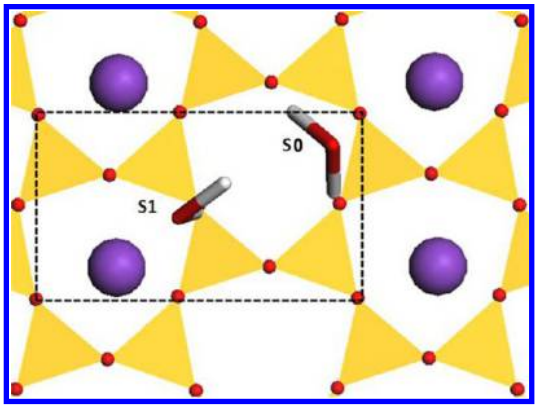

Figure 12. Two configurations of water molecules adsorbed on two different binding sites, S0 (corresponding to L0) and S1 (corresponding to L1), on the mica surface. K^+ is in purple, O is in red. The polyhedron contains silicon or aluminum at its center.

to molecules in L1. Figure 12 also shows that S0 forms two hydrogen bonds (these two hydrogen bonds are not exactly the same, one is slightly longer than another), S1 forms one hydrogen bond, and oxygen atoms from water interact with K^+ cation over a short distance. The energy differences between these two configurations were calculated using the force field method. The result shows that the binding energy to the surface is 10 kJ/mol stronger for the S1 molecule than that for the S0 molecule, which is in reasonable agreement with the data of 12 kJ/mol calculated using the CPMD method.[4]

Figure 13 shows the order parameters calculated for ethanol. The definition of the order parameter is the same as that used in pure ethanol. The data are calculated for systems with RH ranging from 10% to 90%. The ethanol molecules at low RH are mostly populated in L1 and L2 (see Figure 10), thus, the uncertainty is high at long distances (L3). Most ethanol molecules at high RH are in L2 and L3, thus, the uncertainty is large at short distances (L1). Nevertheless, the order parameters are positive at short distances (L1) and negative between 0.30 and 0.40 nm (L2); both are similar to those obtained for pure ethanol. However, differences are obvious in the range of 0.4 and 0.6 nm (L3). This region of pure ethanol is in the vapor phase, where the order parameters are scattered with large noise but average about zero. This region in the ethanol/water mixture is in the adsorbed ethanol-rich domain, where the structure factors are at low (ca. 0.3) positive values, indicating that the top layer of ethanol molecules are in loosely lined up configurations with hydrogen bonds with the underlying water-rich domain and that the tails of ethanol are oriented toward the vapor phase. The order parameters are scatted at above 0.6 nm of the vapor phase.

The lower values of the structure factors for ethanol in L3 also indicate that the ethanol-rich domain is somewhat randomized with liquid-like features. This observation is supported by the calculated mobility of ethanol on the surface. The two-dimensional lateral diffusion coefficient of ethanol is $(2.0 \pm 0.4 \times 10^{-5})$ cm^2/s, which is nearly the same as that of an aqueous ethanol solution[52] and an order of magnitude higher than that of ethanol at the ethanol/mica interface $((3.0 \pm 0.1) \times 10^{-4}$ $cm^2/s)$.

A snapshot of the simulated water/ethanol/mica interface is shown in Figure 14. The snapshot is a side view of the adsorption interface with very high humidity (RH = 98%), and provides a visual description for the data discussed above. Figure 14 shows that the water-rich domain is in direct contact with the mica surface. The first layer of water (L0) is at the same distance from the surface as that of potassium cations (K^+, the purple balls). The water-rich layer is about two molecular dimensions thick, and contains a small number of ethanol molecules. The ethanol-rich domain is on top of the water-rich domain. Although ethanol molecules are irregularly oriented, most ethanol molecules are oriented head-down and hydrogen-bonded with the water-rich domain and tail-up toward the vapor. Another interesting feature of the snapshot is that at high RH (98%), additional ethanol molecules are adsorbed thereby

dx.doi.org/10.1021/jp3020595 | J. Phys. Chem. C 2012, 116, 16436−16446

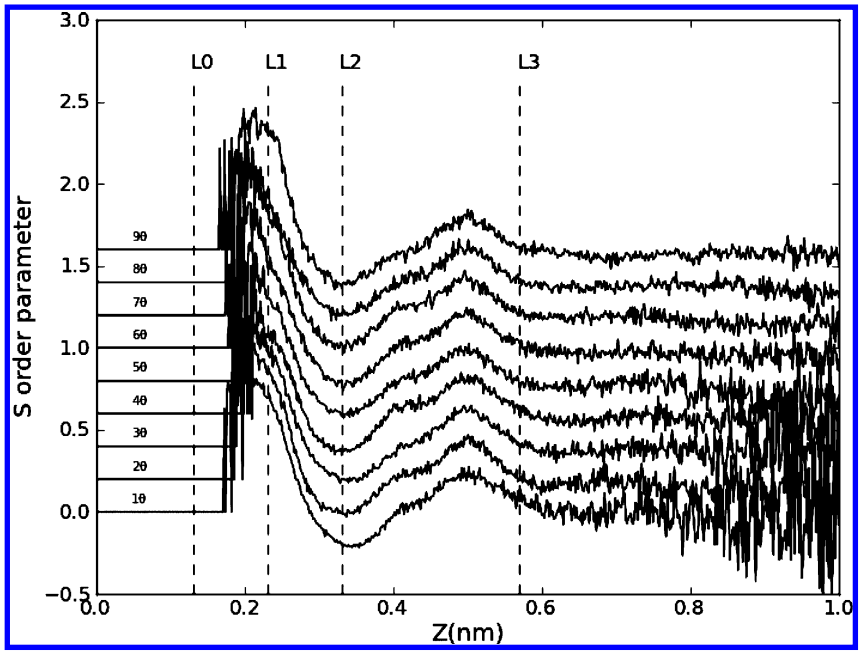

Figure 13. Order parameters between the H−O of ethanol and the *z*-axis as a function of distances from the surface, at various RH values between 10% and 90%. The positions of L0, L1, L2, and L3 are labeled as dashed vertical lines for viewing convenience. The curves calculated at different vapor pressures are shifted along the *y*-axis for better viewing.

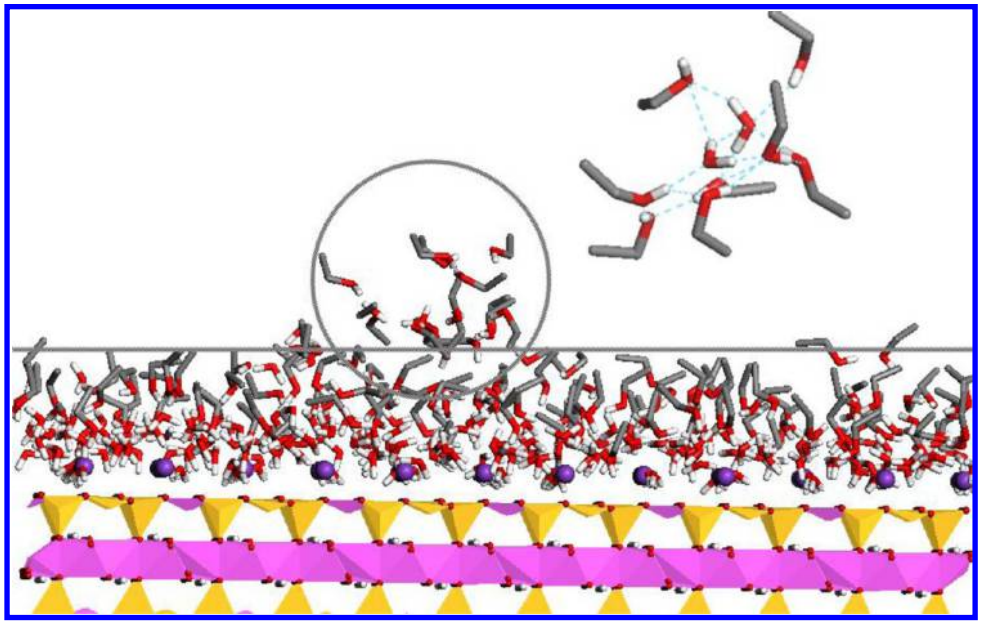

Figure 14. Snapshot of the ethanol adsorption (RH = 98%, ethanol p/p_0 = 90%). The circle emphasizes the cluster structure (ethanol centered with water) on the ethanol monolayer. The enlarged cluster structure is displayed for easy viewing. The hydrogen bond in the structure is shown by the slashed cyan line.

recovering the number of adsorbed ethanol molecules (Figure 8). However, these molecules form clusters with water molecules on the surface, instead of forming a new ethanol layer, as circled out in the figure.

Although L0 is populated with water and K^+, the hydration of K^+ cations is not by water from L0, but from L1 and L2. In this study, the radial distribution function (RDF) between K+ and the oxygen atoms of water and ethanol was calculated, and the results are shown in Figure 15. The RDFs are calculated by counting O from water or O from ethanol from selected layers. Figure 15 shows that the hydration of K^+ cations mainly comes from the L1 and L2 of water and ethanol. All of these RDFs show a peak around 0.28 nm, corresponding to the hydration radius of K^+ cations. The RDF for L0 water peaks at a much longer distance (about 0.5 nm), which can be understood by viewing the two configurations illustrated in Figure 12. The S0 water (L0) is fixed on the surface by forming two hydrogen bonds with the surface. The distance of its oxygen is farther apart from K+, but the S1 molecule (L1) has only hydrogen bonded to the surface, and the water oxygen interacts with the K+ over a shorter distance.

dx.doi.org/10.1021/jp3020595 | *J. Phys. Chem. C* 2012, 116, 16436−16446

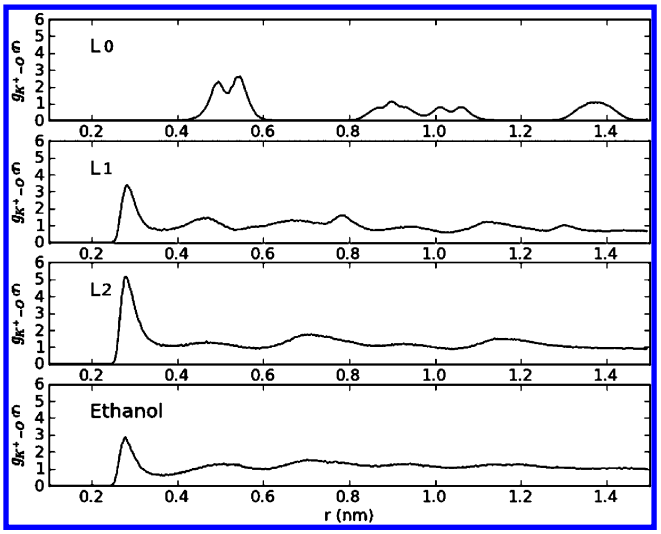

Figure 15. In plane K^+−O 2D (X−Y) radial distribution functions of different layers of water (L0, L1, and L2) and ethanol.

The calculated isosteric heats of adsorption indicate that both water and ethanol interact strongly with the mica surface. The heats of vaporization are similar between water and ethanol (38−40 kJ/mol),[32,40] and the interaction between the two molecules are of about the same amplitude. Therefore, segregation to water-rich and ethanol-rich domains does not occur in the liquid state. The free energy difference induced by the surface is the driving force of the segregation on the surface. The water in the region near the mica surface, as shown by the density distribution (Figure 9), populates at the same distance level of K^+, but the closest distance to the surface for ethanol is about 1 Å above the K^+. Water not only accesses more space on the surface but also adopts more configurations due to its smaller dimensions. Therefore, an entropy contribution that favors water occupying the space closest to the mica surface is observed. Adsorbed water provides hydrogen bond donors and acceptors for additional adsorbates that further lower the total energy of the interface, as discussed above. Alternative placement (the ethanol adsorbed in the first layer) does not provide such enthalpy reduction.

The finding of a multilayer water-rich domain covered by a monolayer ethanol-rich domain provides additional information on a recent Vibrating Scanning Polarization Force Microscopy experimental study[53] in which the authors speculated that ethanol molecules are located on top of the water layer. Although the simulation results cannot be directly compared with the VSPFM pictures, the surface properties modulated by ethanol provide further insights that may help researchers understand the experimental observations. For example, measurement of the surface tension may provide useful information. The concentration of ethanol on the top layer corresponds to a surface concentration of 7.2×10^{-10} mol·cm^{-2}, which is about 11% higher than the maximum surface concentration (6.5×10^{-10} mol/cm^2) of ethanol in aqueous ethanol solutions.[29] Considering that the surface tension of aqueous ethanol solution is 23 mN/m at the maximum surface concentration,[29] we speculate that the surface tension of ethanol-covered interface on the mica surface should be even lower than the aqueous ethanol solutions.

4. CONCLUSION

The simulations revealed a sharp difference between water vapor and ethanol vapor adsorbed on the mica surface, in which the former forms a multilayer, whereas the latter forms a monolayer. The difference is essentially due to the difference in the number of hydrogen bonds that may be formed between these two molecules. On the mica surface, the adsorbed water may continue to function as a hydrogen-bond acceptor and donor, but the adsorbed ethanol does not. To the best of our knowledge, no direct experimental work for ethanol vapor adsorption without humidity is available for comparison with our work. Nevertheless, the experimental data[51,52] measured for ethanol vapor adsorbed on the ice surface supports our conclusion.

The segregation of water-rich and ethanol-rich domains on the mica surface was observed for the mixture adsorption. The segregation does not occur in bulk because both molecules are very similar in cohesive energies. However, segregation occurs on the surface because of the differences in adsorbed structures and positions. In addition, the water-rich domain is generally multilayer in nature, except at extremely low RH (<1%), whereas the ethanol-rich domain exists a monolayer and lies on the top of the water-rich domain.

■ ASSOCIATED CONTENT

Ⓢ Supporting Information

The structural analysis of pure water adsorption on mica is shown in the Supporting Information, including its density profile and S order parameter. This material is available free of charge via the Internet at http://pubs.acs.org.

■ AUTHOR INFORMATION

Corresponding Author

*Tel.: +86-21-5474-8987. Fax: +86-21-5474-1297. E-mail: huaisun@sjtu.edu.cn.

Notes

The authors declare no competing financial interest.

■ ACKNOWLEDGMENTS

This work was stimulated by discussions with Dr. Donghua Zhang, who performed the VSPFM measurements of vapor/water ethanol on mica surface. The authors are grateful to the National Science Foundation of China (Nos. 21073119 and 21173146) and the National Basic Research Program of China (No. 2007CB209701) for their financial support.

■ REFERENCES

(1) Verdaguer, A.; Sacha, G. M.; Bluhm, H.; Salmeron, M. *Chem. Rev.* **2006**, *106*, 1478−1510.
(2) Ewing, G. E. *Chem. Rev.* **2006**, *106*, 1511−1526.
(3) Hu, J.; Xiao, X.-D.; Ogletree, D. F.; Salmeron, M. *Science* **1995**, *268*, 267−269.
(4) Odelius, M.; Bernasconi, M.; Parrinello, M. *Phys. Rev. Lett.* **1997**, *78*, 2855−2858.
(5) Yaminsky, V.; Ninham, B.; Karaman, M. *Langmuir* **1997**, *13*, 5979−5990.
(6) Miranda, P. B.; Xu, L.; Shen, Y. R.; Salmeron, M. *Phys. Rev. Lett.* **1998**, *81*, 5876−5879.
(7) Xu, L.; Lio, A.; Hu, J.; Ogletree, D. F.; Salmeron, M. *J. Phys. Chem. B* **1998**, *102*, 540−548.
(8) Cantrell; Ewing, G. E. *J. Phys. Chem. B* **2001**, *105*, 5434−5439.
(9) Cheng, L.; Fenter, P.; Nagy, K. L.; Schlegel, M. L.; Sturchio, N. C. *Phys. Rev. Lett.* **2001**, *87*, 156103.

(10) Al-Abadleh, H. A.; Grassian, V. H. *Langmuir* **2002**, *19*, 341−347.
(11) Park, S.-H.; Sposito, G. *Phys. Rev. Lett.* **2002**, *89*, 085501.
(12) Spagnoli, C.; Loos, K.; Ulman, A.; Cowman, M. K. *J. Am. Chem. Soc.* **2003**, *125*, 7124−7128.
(13) Leng, Y.; Cummings, P. T. *Phys. Rev. Lett.* **2005**, *94*, 026101.
(14) Wang, J.; Kalinichev, A. G.; Kirkpatrick, R. J.; Cygan, R. T. *J. Phys. Chem. B* **2005**, *109*, 15893−15905.
(15) Balmer, T. E.; Christenson, H. K.; Spencer, N. D.; Heuberger, M. *Langmuir* **2007**, *24*, 1566−1569.
(16) Meleshyn, A. *J. Phys. Chem. C* **2008**, *112*, 20018−20026.
(17) Meleshyn, A. *J. Phys. Chem. C* **2008**, *112*, 14495−14500.
(18) Meleshyn, A. *J. Phys. Chem. C* **2009**, *113*, 17604−17607.
(19) Fukuma, T.; Ueda, Y.; Yoshioka, S.; Asakawa, H. *Phys. Rev. Lett.* **2010**, *104*, 016101.
(20) Kimura, K.; Ido, S.; Oyabu, N.; Kobayashi, K.; Hirata, Y.; Imai, T.; Yamada, H. *J. Chem. Phys.* **2010**, *132*, 194705−194709.
(21) Teschke, O.; Filho, J. F. V.; de Souza, E. F. *Chem. Phys. Lett.* **2010**, *485*, 133−136.
(22) Romero-Vargas Castrillón, S.; Giovambattista, N. s.; Aksay, I. A.; Debenedetti, P. G. *J. Phys. Chem. C* **2011**, *115*, 4624−4635.
(23) Delville, A. *J. Phys. Chem.* **1995**, *99*, 2033−2037.
(24) Cygan, R. T.; Liang, J.-J.; Kalinichev, A. G. *J. Phys. Chem. B* **2004**, *108*, 1255−1266.
(25) Malani, A.; Ayappa, K. G. *J. Phys. Chem. B* **2009**, *113*, 1058−1067.
(26) Du, Z.; Manos, G.; Vlugt, T. J. H.; Smit, B. *AIChE J.* **1998**, *44*, 1756−1764.
(27) Donaldson, D. J.; Anderson, D. *J. Phys. Chem. A* **1999**, *103*, 871−876.
(28) Müller, E. A.; Hung, F. R.; Gubbins, K. E. *Langmuir* **2000**, *16*, 5418−5424.
(29) Stewart, E.; Shields, R. L.; Taylor, R. S. *J. Phys. Chem. B* **2003**, *107*, 2333−2343.
(30) Sung, J.; Park, K.; Kim, D. *J. Phys. Chem. B* **2005**, *109*, 18507−18514.
(31) Garrett, B. C.; Schenter, G. K.; Morita, A. *Chem. Rev.* **2006**, *106*, 1355−1374.
(32) Glattli, A.; Daura, X.; Gunsteren, W. F. v. *J. Chem. Phys.* **2002**, *116*, 9811−9828.
(33) Lowell, S. *Characterization of Porous Solids and Powders: Surface Area, Pore Size, and Density*; Kluwer Academic Publishers, Norwell, MA, 2004.
(34) Zhang, L.; Liu, W.; Shen, Y. R.; Cahill, D. G. *J. Phys. Chem. C* **2007**, *111*, 2069−2076.
(35) Fang, Y.; Hoh, J. H.; Spisz, T. S. *Nucleic. Acids. Res.* **1999**, *27*, 1943−1949.
(36) Zhang, C.; van der Maarel, J. R. C. *J. Phys. Chem. B* **2008**, *112*, 3552−3557.
(37) Knurr, R. A.; Bailey, S. W. *Clay Clay Miner.* **1986**, *34*, 7−16.
(38) Pullman, B. Intermolecular forces. Proceedings of the 14th Jerusalem Symposium on Quantum Chemistry and Biochemistry, Jerusalem, Israel, April 13−16, 1981; D. Reidel: Dordrecht, The Netherlands, 1981.
(39) Chen, B.; Potoff, J. J.; Siepmann, J. I. *J. Phys. Chem. B* **2001**, *105*, 3093−3104.
(40) Rai, N.; Wagner, A. J.; Ross, R. B.; Siepmann, J. I. *J. Chem. Theory Comput.* **2007**, *4*, 136−144.
(41) Rowley, L. A.; Nicholson, D.; Parsonage, N. G. *J. Comput. Phys.* **1975**, *17*, 401−414.
(42) Liu, J. C.; Monson, P. A. *Langmuir* **2005**, *21*, 10219−10225.
(43) Siepmann, J. I.; Frenkel, D. *Mol. Phys.* **1992**, *75*, 59−70.
(44) Hess, B.; Kutzner, C.; van der Spoel, D.; Lindahl, E. *J. Chem. Theory Comput.* **2008**, *4*, 435−447.
(45) Berendsen, H. J. C.; Postma, J. P. M.; Gunsteren, W. F. v.; DiNola, A.; Haak, J. R. *J. Chem. Phys.* **1984**, *81*, 3684−3690.
(46) Darden, T.; York, D.; Pedersen, L. *J. Chem. Phys.* **1993**, *98*, 10089−10092.
(47) Egberts, E.; Berendsen, H. J. C. *J. Chem. Phys.* **1988**, *89*, 3718−3732.
(48) Snurr, R. Q.; Bell, A. T.; Theodorou, D. N. *J. Phys. Chem.* **1993**, *97*, 13742−13752.
(49) Zhuo, Bo.; Wang, Chun-Lei; Xiu, Peng; Fang, Hai-Ping. *Commun. Theor. Phys.* **2012**, *57*, 308.
(50) Wang, L.; Song, Y.; Zhang, B.; Wang, E. *Thin Solid Films* **2004**, *458*, 197−202.
(51) Schnabel, T.; Vrabec, J.; Hasse, H. *Fluid Phase Equilib.* **2005**, *233*, 134−143.
(52) Guevara-Carrion, G.; Vrabec, J.; Hasse, H. *J. Chem. Phys.* **2011**, *134*, 074508.
(53) Zhang, D.; Zhang, C.; Zhang, F.; Hu, J. *Microsc. Res. Tech.* **2011**, *74*, 481−483.